Subcellular calcium dynamics in a whole-cell model of an atrial myocyte

Rüdiger Thul[a,1], Stephen Coombes[a], H. Llewelyn Roderick[b,c], and Martin D. Bootman[b]

[a]School of Mathematical Sciences, University of Nottingham, Nottingham NG7 2RD, United Kingdom; [b]Laboratory of Signalling and Cell Fate, The Babraham Institute, Babraham, Cambridge CB22 3AT, United Kingdom; and [c]Department of Pharmacology, University of Cambridge, Cambridge CB2 1PD, United Kingdom

Edited by Michael J. Berridge, The Babraham Institute, Cambridge, United Kingdom, and approved December 22, 2011 (received for review September 30, 2011)

In this study, we present an innovative mathematical modeling approach that allows detailed characterization of Ca^{2+} movement within the three-dimensional volume of an atrial myocyte. Essential aspects of the model are the geometrically realistic representation of Ca^{2+} release sites and physiological Ca^{2+} flux parameters, coupled with a computationally inexpensive framework. By translating nonlinear Ca^{2+} excitability into threshold dynamics, we avoid the computationally demanding time stepping of the partial differential equations that are often used to model Ca^{2+} transport. Our approach successfully reproduces key features of atrial myocyte Ca^{2+} signaling observed using confocal imaging. In particular, the model displays the centripetal Ca^{2+} waves that occur within atrial myocytes during excitation–contraction coupling, and the effect of positive inotropic stimulation on the spatial profile of the Ca^{2+} signals. Beyond this validation of the model, our simulation reveals unexpected observations about the spread of Ca^{2+} within an atrial myocyte. In particular, the model describes the movement of Ca^{2+} between ryanodine receptor clusters within a specific z disk of an atrial myocyte. Furthermore, we demonstrate that altering the strength of Ca^{2+} release, ryanodine receptor refractoriness, the magnitude of initiating stimulus, or the introduction of stochastic Ca^{2+} channel activity can cause the nucleation of proarrhythmic traveling Ca^{2+} waves. The model provides clinically relevant insights into the initiation and propagation of subcellular Ca^{2+} signals that are currently beyond the scope of imaging technology.

A human heart beats more than a billion times during the average lifespan, and is required to do so with great fidelity. The ventricular chambers of the heart are responsible for generating the force that propels blood to the lungs and body (1). Under sedentary conditions, the atrial chambers make only a minor contribution to blood pumping. However, during periods of increased hemodynamic demand, such as exercise, atrial contraction increases to enhance the amount of blood within the ventricles before they contract. This "atrial kick" is believed to account for up to 30% extra blood-pumping capacity. Deterioration of atrial myocytes with aging causes the loss of this blood-pumping reserve, thereby increasing frailty in the elderly. Atrial kick is also lost during atrial fibrillation (AF), the most common form of cardiac arrhythmia. The stagnation of blood within the atrial chambers during AF can cause thrombus formation, leading to thromboembolism. Approximately 15% of all strokes occur in people with AF. As shown in numerous reports, the genesis and maintenance of AF is causally linked to the dysregulation of Ca^{2+} signaling (2–4). Detailed characterization of Ca^{2+} movement within atrial myocytes is therefore necessary to understand changes involved in aging and conditions such as AF.

Elevation of the cytosolic Ca^{2+} concentration is the trigger for contraction of cardiac myocytes (1). Engagement of Ca^{2+} with troponin C (TnC) allows the actin and myosin filaments to interact and slide past each other, thereby causing cell shortening. The sequence of events that leads to a Ca^{2+} rise during excitation–contraction coupling (EC coupling) is well-known. Essentially, depolarization of cardiac myocytes activates voltage-operated Ca^{2+} channels (VOCs) that allow the entry of Ca^{2+} from the extracellular space. This Ca^{2+} influx signal is greatly amplified via a process known as Ca^{2+}-induced Ca^{2+} release (CICR) by intracellular Ca^{2+} channels (ryanodine receptors; RyRs) expressed on the sarcoplasmic reticulum (SR). The SR membrane bearing RyRs comes within 10 nm of the sarcolemma, thereby forming compartments known as "dyadic junctions" in which CICR rapidly occurs. Mammalian ventricular myocytes have an extensive series of sarcolemmal invaginations (T tubules) that bring VOCs and RyRs into close proximity within dyadic junctions throughout the volume of the cells. Each dyadic junction produces an elementary Ca^{2+} signal known as a "Ca^{2+} spark" during EC coupling. The spatial overlap of many thousands of Ca^{2+} sparks gives rise to the homogeneous Ca^{2+} signals associated with ventricular EC coupling.

In contrast, the atrial myocytes of many mammalian species do not express extensive T-tubule networks. In this situation, the coupling of VOCs and RyRs occurs at dyadic junctions around the periphery of the cells. The consequence of this arrangement is that Ca^{2+} signals originate around the edge of atrial myocytes during EC coupling (2). We, and others, have shown that under resting conditions this peripheral Ca^{2+} signal does not propagate into the center of atrial cells, so that at the peak of the response substantial Ca^{2+} gradients can be observed from a cell's edge to its center (5–7). However, in addition to the junctional RyRs that are activated at the onset of EC coupling, atrial myocytes express clusters of RyRs in a regular three-dimensional lattice throughout their volume. It could be expected that these nonjunctional RyRs would sense the subsarcolemmal Ca^{2+} signal and convey it deeper into a cell via CICR. Indeed, to trigger substantial contraction, the Ca^{2+} wave must move toward the center of an atrial cell, because the extent of inward movement of the Ca^{2+} wave and atrial myocyte contraction are linearly related (8, 9). The nonjunctional RyRs therefore appear to act as an inotropic reserve that becomes active under conditions where greater atrial contraction is required. Little is known about the mechanisms that control the propagation of Ca^{2+} between RyRs within atrial myocytes.

In the present study, we characterized the movement of Ca^{2+} during EC coupling in an idealized atrial myocyte model. The model describes a three-dimensional lattice of discrete Ca^{2+} release sites that equate in position and function to those within a living atrial cell. Our method, which translates key properties of cellular Ca^{2+} transport into a framework of significantly low computational overhead, allows the activity of all of the discrete

Author contributions: R.T., S.C., H.L.R., and M.D.B. designed research; R.T., S.C., and M.D.B. performed research; R.T. and M.D.B. analyzed data; and R.T. and M.D.B. wrote the paper.

The authors declare no conflict of interest.

This article is a PNAS Direct Submission.

Freely available online through the PNAS open access option.

[1]To whom correspondence should be addressed. E-mail: ruediger.thul@nottingham.ac.uk.

This article contains supporting information online at www.pnas.org/lookup/suppl/doi:10.1073/pnas.1115855109/-/DCSupplemental.

Ca^{2+} release sites to be *simultaneously* monitored, and for Ca^{2+} signals to be activated at any particular site(s). We provide an overview of the model in *Materials and Methods*, and refer the reader to *SI Materials and Methods*, for a detailed discussion of our modeling approach.

The model was validated by replicating known properties of atrial myocyte Ca^{2+} signaling, such as the centripetal diffusion of Ca^{2+} from the periphery of an atrial myocyte to the cell center. Moreover, the model allows us to explore factors critical to the fidelity of Ca^{2+} signaling that cannot be manipulated experimentally. Although our simulations used the geometry of an atrial myocyte without T tubules, our findings are also relevant to other myocytes that do not possess T tubules (e.g., neonatal myocytes). Furthermore, T tubules in mature ventricular myocytes are lost during aging or under disease conditions. In situations where T tubules are lost, EC coupling is initiated around the periphery of the cells and contraction will be dependent on saltatoric Ca^{2+} wave propagation as for the atrial myocytes described in this study. The arrhythmic calcium wave activity presented herein is relevant to non-tubulated and de-tubulated myocytes.

Results

The aim of this study was to produce a geometrically realistic model of an atrial myocyte. By incorporating the actual positioning of discrete Ca^{2+} release sites, we could explore their interaction and involvement in Ca^{2+} wave initiation and propagation. Based on empirical measurements of RyR distribution from numerous studies (2) (Fig. 1*A*), we modeled an atrial myocyte as a cylinder 100 μm in length and 12 μm in diameter, as depicted in Fig. 1*B*. Within the cylinder, Ca^{2+} release was constrained to 51 two-dimensional disks situated perpendicular to the long axis of the cylinder, and spaced 2 μm apart. These disks correspond to the z planes within atrial myocytes where the RyRs are expressed (8, 10, 11) (Fig. 1*A*). Within the z planes, the Ca^{2+} release sites were distributed as shown in Fig. 2*A*. The outermost ring of Ca^{2+} release sites represents the junctional RyRs that face the VOCs in dyadic junctions, whereas the inner Ca^{2+} release sites equate to nonjunctional RyRs. The radial

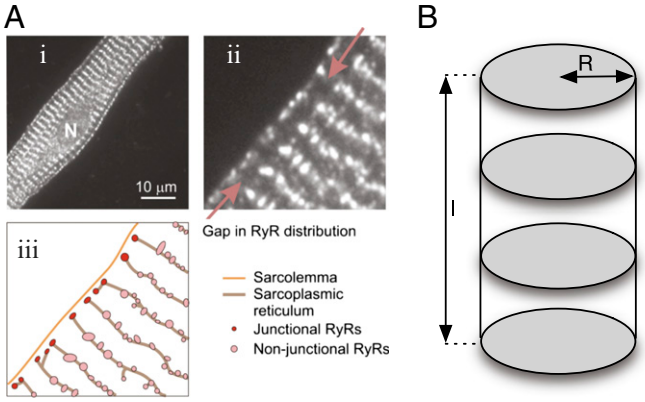

Fig. 1. (*A*) Distribution of type 2 RyRs in an atrial myocyte immunostained with an anti-type 2 RyR antibody. (*i*) A portion of an atrial myocyte. The transverse striations of nonjunctional RyRs, and peripheral junctional RyRs are evident. "N" denotes the position of the nucleus. (*ii*) An enlarged section of the same cell. The gap in RyR distribution between the junctional RyRs and the nonjunctional RyRs is indicated by arrows. (*iii*) A cartoon representation of the arrangement of RyRs and cellular membranes relating to *ii*. The position of the RyR clusters was determined by thresholding the image in *ii* so that all positive pixels in the background were absent, and then identifying the remaining areas with positive fluorescence. (*B*) Cylindrical atrial myocyte geometry used in simulations showing a stack of z planes. The location of individual clusters within a disk is illustrated in Fig. 2*A*.

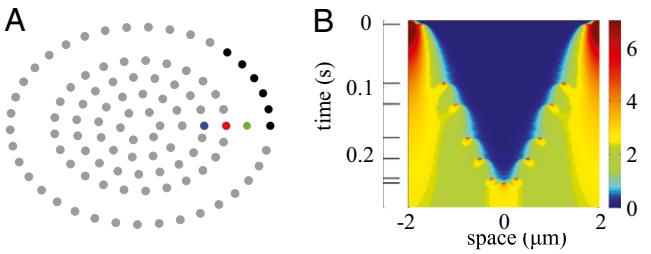

Fig. 2. (*A*) Position of Ca^{2+} release sites within a single z plane as used in the simulations. See text for details concerning the colors. (*B*) Space–time plot of a one-dimensional saltatory propagating wave. Parameter values are $\tau = 1$ s, $D = 1\ \mu m^2 \cdot s^{-1}$, $c_{th} = 1$ μM, and $\sigma = 0.26$ μM. The bars on the left indicate the time of successive release Ca^{2+} events.

distance between the rings of nonjunctional Ca^{2+} release sites is 1 μm (Fig. 2*A*). Between the junctional Ca^{2+} release sites and the first ring of nonjunctional Ca^{2+} release sites is a spacing of 2 μm, reflecting the gap of RyR expression observed in atrial myocytes (Fig. 1*Aii*). The spacing of Ca^{2+} release sites around each ring is 1 μm. This model allows us to investigate the movement of Ca^{2+} within one, two, or three dimensions, and to examine interactions between Ca^{2+} release sites within the same, or neighboring, z planes.

Deterministic Release. Movement of Ca^{2+} within the model relies on saltatory wave propagation involving discrete Ca^{2+} release sites. A one-dimensional representation of such a wave, obtained analytically, is shown in Fig. 2*B* (details will be published elsewhere). A centripetal Ca^{2+} wave travels from the periphery to the center of the cell. The propagation rate and amplitude of the Ca^{2+} wave in the full three-dimensional cell model both diminish as it moves inwardly. Essentially, Ca^{2+} diffusing between successive release sites has to overcome the continual inhibitory effect of sarcoendoplasmic reticulum Ca^{2+} ATPases (SERCAs), and as the Ca^{2+} signal diminishes it takes longer to initiate Ca^{2+} release at the next RyR cluster. It is already established that RyR activity is regulated by a range of factors including luminal Ca^{2+}, phosphorylation, accessory proteins, and accessory factors. To simplify the model, we convolved the effect of these factors in two key parameters—release strength and release threshold. These parameters encompass possible changes in the total Ca^{2+} flux through a cluster of RyRs and RyR sensitivity irrespective of the molecular mechanism. Saltatory wave propagation critically depends on release strength and threshold. If the release strength is too small, or the threshold is too high, then Ca^{2+} waves cannot propagate.

We next examined the movement of Ca^{2+} within a single z plane. Ca^{2+} release was initiated by activating the six peripheral Ca^{2+} release sites colored black in Fig. 2*A*. The black curve in Fig. 3*A* illustrates the profile of the Ca^{2+} signal at those peripheral sites. The red, blue, and green curves depict the time courses of Ca^{2+} concentration at Ca^{2+} release sites deeper inside the cell (denoted by corresponding colors in Fig. 2*A*). Because we trigger release at the periphery, we observe an immediate response in that location. The next release site (red) opens with some latency, and the peak amplitude is damped in comparison with the outer release site. Moving further toward the interior of the cell, Ca^{2+} release begins even later, while peak values continue to decrease. The sharp rise and fall of the concentration profiles is a combined effect of the threshold dynamics of release in a 3D volume and the impact of SERCA pumps. Reducing the release strength leads to overall smaller Ca^{2+} profiles and slowing of saltatoric Ca^{2+} wave propagation, but the tendency of growing latencies and smaller maxima for inner release sites remains unchanged (compare Fig. 3 *A* and *B*). Note that a

PHYSIOLOGY

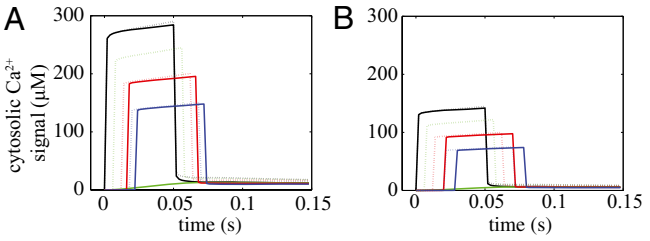

Fig. 3. Time course of the Ca^{2+} concentration for σ = 90 μM·μm^3·s^{-1} (*A*) and σ = 45 μM·μm^3·s^{-1} (*B*) in the central z plane at θ = 0 and r = 5.9 μm (black), r = 4.9 μm (green), r = 3.9 μm (red), and r = 2.9 μm (blue) in the presence (solid lines) and absence (dotted lines) of a diffusive gap. Parameter values are as in Table S1 and dt = 0.002 s.

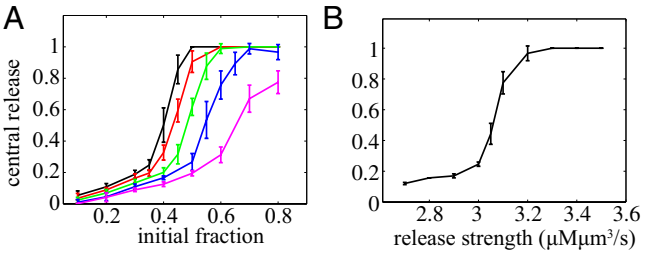

Fig. 4. Mean relative response and variance (error bars) of the central cylinder of release sites (r = 0.9 μm) as a function of initial fraction (*A*) and varying Ca^{2+} release strength σ (*B*). Parameter values are (*A*) σ = 3.5 (black), 3.4 (red), 3.3 (green), 3.2 (blue), 3.1 μM·μm^3·s^{-1} (magenta). (*B*) The initial fraction is 0.8. All other parameter values are as in Table S1 and t_{ref} = 1 s.

release strength of 45 μM·μm^3·s^{-1} corresponds to ∼400 open RyRs when we assume a single channel current of 1 pA.

An aspect of atrial myocyte ultrastructure that we considered at this point was the effect of the gap in Ca^{2+} release sites between the junctional RyRs and the first ring of nonjunctional RyRs. As depicted in Fig. 2*A*, the spacing between rings of Ca^{2+} release sites is 1 μm inside the cell, with a 2 μm gap to the peripheral junctional ring of Ca^{2+} release sites. The 2 μm gap was adopted into the model because studies have shown such a discontinuity in the expression of RyR clusters (10, 12, 13). The physiological reason for this gap in atrial RyR distribution is not known. We observed that for minimal release strengths the gap prevented the inward propagation of the Ca^{2+} wave, such that only the peripheral Ca^{2+} release sites were active (Fig. S1).

The consequence of incorporating an additional ring of Ca^{2+} release sites (green release site in Fig. 2*A*) within the gap between the junctional and nonjunctional RyRs is depicted in Fig. 3. The essential effect of the additional Ca^{2+} release sites was to accelerate the centripetal propagation of the Ca^{2+} wave by reducing the distance over which Ca^{2+} had to diffuse before attaining a threshold concentration for CICR. These data suggest that the gap in RyR distribution imparts a natural barrier to hinder Ca^{2+} movement. This is likely to be a physiological mechanism for limiting atrial contraction under resting conditions.

The magnitude of atrial myocyte contraction is determined by the distance that the centripetal Ca^{2+} wave is able to spread (2, 8). This is due to the increasing recruitment of myofilaments as Ca^{2+} waves progress deeper into an atrial cell. The extent of propagation of the centripetal wave is modulated by application of positive inotropic hormones such as endothelin-1 or β-adrenergic agonists (8, 14).

To measure the effect of positive inotropic stimulation in our model, we determined the activity of Ca^{2+} release sites within the innermost rings (r = 0.9 μm) of all 51 z planes. For those release sites to be activated, Ca^{2+} has to travel in a saltatoric manner from the periphery of the cell, as described above. We varied the degree of cell stimulation by altering the fraction of peripheral Ca^{2+} release sites that were activated at the inception of a response (hereafter denoted "initial fraction"; the actual position of those sites was randomly assigned). The black curve in Fig. 4*A* depicts the increasingly successful recruitment of central Ca^{2+} release sites as the initial fraction was progressively enhanced. The data show that for strong stimulation, that is, for a large initial fraction, almost all release sites in the innermost rings become activated. On the other hand, a lesser initial fraction elicits a considerably damped response in the center.

An unexpected outcome was that the variance of central channel opening was not uniform. Generally, triggering either relatively few, or many, peripheral Ca^{2+} release sites gave consistent responses (small error bars on the curves in Fig. 4*A*), whereas activating an intermediate number of peripheral Ca^{2+} release sites gave more variable penetration into the cell (large error bars). The error bars indicate that not all triggered responses, even with the same number of initiating Ca^{2+} release sites, resulted in the same degree of centripetal Ca^{2+} wave propagation. The key point of this observation is that Ca^{2+} waves sometimes propagate into the cell center but at other times fail, even though they were triggered by the same number of peripheral release sites. This implies that the positions of the initiating sites are critical. Evidently, some configurations of initial calcium release sites fail to nucleate calcium waves. However, the same number of initiating sites, but in a different spatial configuration, can activate a centripetal calcium wave. Interestingly, we have previously observed that atrial myocytes use the same spatial distribution of initiating release sites with each beat [so-called eager sites (13)], thereby avoiding beat-to-beat variability in Ca^{2+} wave nucleation.

Varying the release strength alters the dependency of centripetal Ca^{2+} wave propagation on the initial fraction (colored curves in Fig. 4*A*). Essentially, for lesser release strengths, a greater initiating fraction of Ca^{2+} release sites is required to trigger centripetal Ca^{2+} wave propagation. The steep relationship between recruitment of the innermost Ca^{2+} release sites and strength of Ca^{2+} liberation with fixed initial fraction (0.5) is depicted in Fig. 4*B*. In addition to the positive inotropic effects of increased release strength and increased initial fraction, decreasing the threshold for Ca^{2+} release also promoted centripetal Ca^{2+} waves, and would therefore be positively inotropic (Fig. S2). A comparison of the effects of increasing release strength, increasing initial fraction, and decreasing threshold is depicted in Fig. S3. It is evident that altering any of the parameters could independently enhance centripetal Ca^{2+} wave propagation, but the effects of each parameter were not exactly alike. Increasing the initial fraction or decreasing the threshold for Ca^{2+} release promoted centripetal Ca^{2+} wave propagation and increased the global amplitude of pacing-evoked Ca^{2+} signals. However, the degree of Ca^{2+} signal enhancement was significantly greater if the Ca^{2+} release strength was increased. Essentially, increasing the release strength is the only parameter that actually adds more Ca^{2+} to the system. The other two parameters, initial fraction and threshold, can modulate the ease with which centripetal Ca^{2+} waves can be triggered and propagate, but do not impart any additional Ca^{2+} inside the cell. These analyses suggest that at least three different parameters control the success of Ca^{2+} wave movement within an atrial myocyte, but that release strength, the amount of Ca^{2+} released, is the most potent effector.

The three-dimensional atrial cell model also allows us to explore putative arrhythmic patterns of Ca^{2+} signaling that arise from localized Ca^{2+} release activity. In particular, we examined how Ca^{2+} liberated at one z plane influences Ca^{2+} release sites in neighboring z planes. Such a situation is depicted in Fig. 5*A*, which shows Ca^{2+} waves initiating at the central z plane within

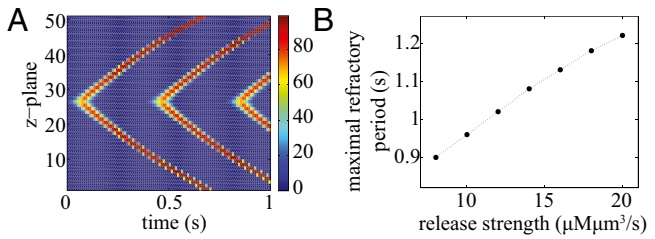

Fig. 5. (*A*) Traveling wave initiated in the central z plane for σ = 90 μM·μm^3·s^{-1} and t_{ref} = 0.34 s. The Ca^{2+} wave was initiated by activating six adjacent peripheral release sites. (*B*) Maximal refractory period as a function of the release strength σ. Colors represent the proportion of open channels in a single z plane.

an atrial myocyte that subsequently propagate to the top and bottom of the cell. The figure shows three traveling Ca^{2+} waves of which only the first one was triggered, and the second and third arose autonomously. The reinitiation of such Ca^{2+} waves occurs if the Ca^{2+} concentration within the z plane that was first triggered is above the threshold for Ca^{2+} release when the RyRs emerge from being refractory. The reinitiation of Ca^{2+} waves reflects an interplay between the processes that serve to introduce Ca^{2+} into the cytoplasm (i.e., Ca^{2+} release strength), the processes that diminish the buildup of Ca^{2+} concentration (i.e., SERCA pumps and Ca^{2+} diffusion), and the refractory period of the Ca^{2+} release sites. Fig. 5*B* depicts the relationship between Ca^{2+} release strength and the maximal refractory period that will sustain Ca^{2+} wave reinitiation. Essentially, as the Ca^{2+} release strength increases, the time window in which Ca^{2+} wave reinitiation can occur also increases. Increasing the time constant of the SERCA pumps and hence weakening Ca^{2+} resequestration also extends the time window for Ca^{2+} wave reinitiation, because it takes longer for the Ca^{2+} concentration to fall below the threshold for any given release strength. In addition to increased release strength triggering arrhythmic Ca^{2+} waves, we observed that dramatically decreasing release strength also promoted autonomous Ca^{2+} signals. Below a critical Ca^{2+} release strength, RyR activity persists indefinitely once it is activated within a particular plane. This can be inferred from the faint bluish horizontal ribbon in Fig. 6*A*. The blue band represents a Ca^{2+} wave that never terminates because the release sites within that plane are never in a simultaneous refractory state. We call this type of activity "ping waves," and within the model such waves are visualized as an elevated Ca^{2+} concentration within two counterrotating sectors of a single z plane (Movie S1). These perpetually rotating ping waves progressively feed Ca^{2+} to neighboring z planes, eventually evoking longitudinal Ca^{2+} waves. Essentially, a low Ca^{2+} release strength causes only a partial recruitment of Ca^{2+} release sites during EC coupling, thereby seeding ping wave activity. The period of a ping wave is much longer than the typical timescale for replenishing the SR after Ca^{2+} release, allowing the SR to return to its rest state before a new rotation of a ping wave is initiated. These observations are pertinent to conditions such as end-stage heart failure, where Ca^{2+} pumping into the SR is low and RyR expression is diminished (hence release strength is decreased) yet the propensity for arrhythmic Ca^{2+} release is high. The reduced Ca^{2+} release strength evident during heart failure would have the consequence of nonuniform RyR refractoriness, thereby leading to the likely triggering of ping waves.

Stochastic Release. In the previous sections, the modeling assumed a uniform threshold for activation of Ca^{2+} release sites. However, ion channels are intrinsically stochastic (15), and within the heart the stochastic activity of RyRs is enhanced by factors such as phosphorylation, association with accessory proteins, and increased SR Ca^{2+} load. To model these effects, we make the threshold for Ca^{2+} release a random variable that fluctuates independently at each release site. Fig. 7 shows the number of open channels in every z plane as a function of time and illustrates how Ca^{2+} wave dynamics changes when threshold noise grows. At small noise levels (Fig. 7*A*), Ca^{2+} wave propagation resembles a deterministic motion, as in Fig. 5. Upon increasing the noise strength, waves emerge spontaneously (Fig. 7*B*). When two waves meet, they annihilate each other because they run into each other's refractory tail. Note that the spontaneously nucleated wave is weaker in the beginning compared with the induced wave, but eventually induces a longitudinal Ca^{2+} wave. Stronger noise leads to more spontaneous waves (Fig. 7*C*). If the noise strength grows beyond a critical value, almost all channels open immediately. This results in a global rise of activity without any traveling wave.

As described above, refractoriness has a calming influence on Ca^{2+} release by preventing repetitive activation of release sites. A long refractory period ensures that Ca^{2+} declines below the threshold for Ca^{2+} release at the end of a response. However, the introduction of noise can negate the effect of refractory periods on the fidelity of Ca^{2+} signaling. In Fig. 7*D*, for example, several successive waves are evident in a simulation using a

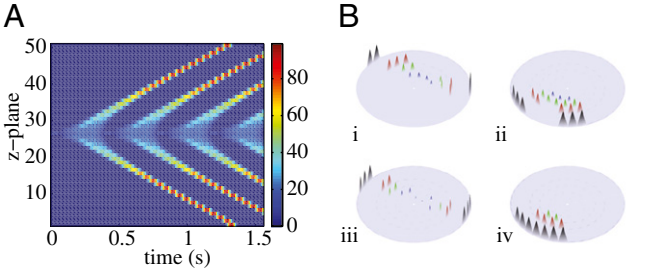

Fig. 6. (*A*) Traveling wave initiated in the central z plane for σ = 7.85 μM·μm^3·s^{-1} and t_{ref} = 0.34 s. The Ca^{2+} wave was initiated by activating six adjacent peripheral release sites. Colors represent the proportion of open channels in a single z plane. (*B*) Ping wave in the central z plane at *t* = 0.18 s (*i*), 0.33 s (*ii*), 0.60 s (*iii*), and 0.75 s (*iv*). The triangular shape of the concentration peaks is for illustration purposes only. Parameter values are as in Table S1.

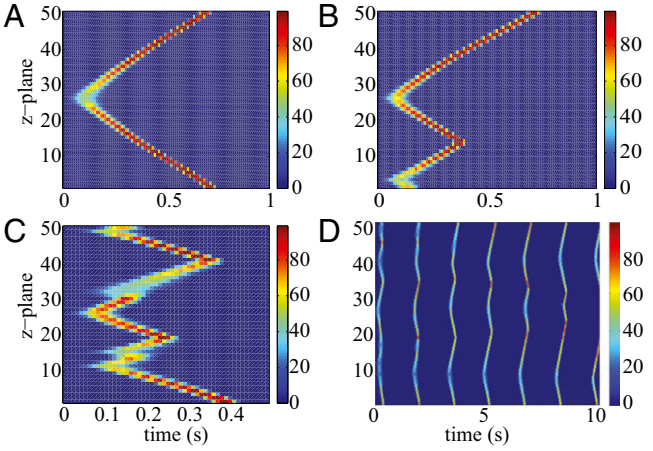

Fig. 7. Traveling wave for σ = 60 μM·μm^3·s^{-1} and β = 200 μM^{-1} (*A*), β = 100 μM^{-1} (*B*), β = 80 μM^{-1} (*C*), and β = 70 μM^{-1} (*D*). The first Ca^{2+} wave was initiated by activating six adjacent peripheral release sites. Parameter values are as in Table S1 and t_{ref} = 1.5 s. Colors represent the proportion of open channels in a single z plane.

PHYSIOLOGY

relatively long refractory period (1.5 s). In the deterministic model with no noise, only the first (triggered) Ca^{2+} wave would be evident. Essentially, introducing noisy thresholds allows some release sites to activate even when Ca^{2+} has recovered to diastolic levels.

Discussion

In the present study, we explored the characteristics of Ca^{2+} movement within an idealized atrial myocyte using a realistic geometrical representation of Ca^{2+} release sites and Ca^{2+} flux values. A key feature of the model is that we can initiate Ca^{2+} release from any of the sites within the three-dimensional lattice and subsequently examine the propagation of the Ca^{2+} signal to other parts. In this way, we could stimulate the peripheral Ca^{2+} release sites to generate a centripetal Ca^{2+} wave (Figs. 2 and 3) that mimics physiological pacing of atrial myocytes during EC coupling (6–8, 16), or activate Ca^{2+} release within the center of the cell to examine the movement of Ca^{2+} waves that would be arrhythmogenic (Figs. 5–7). The propagation of Ca^{2+} signals depends on the diffusion of Ca^{2+} between release sites. If the Ca^{2+} ions released by one site reach the threshold concentration at a neighboring site, then it will be activated and convey the Ca^{2+} signal further.

Atrial myocytes have an essential inotropic function in the heart. The extent of centripetal propagation of a Ca^{2+} wave determines the extent of atrial myocyte contraction. The further a Ca^{2+} wave progresses toward the center of the cell, the more myofilaments become activated (5). The junctional Ca^{2+} release sites are always the first to respond during EC coupling, but by themselves evoke little contraction because the Ca^{2+} signal occurs around the cell periphery. The nonjunctional RyRs therefore represent an inotropic reserve that is activated under conditions when strong contraction is required.

A structural feature of atrial myocytes that may credibly contribute to the peripheral restriction of Ca^{2+} waves is the 2 μm gap in RyR expression between the junctional and nonjunctional Ca^{2+} release sites (Fig. 1). This gap is a particular feature of atrial myocytes, and has been observed in several previous studies (10, 13). Our results indicate that the 2 μm discontinuity in RyR expression significantly hinders the movement of the centripetal Ca^{2+} wave (Fig. 3), because it introduces both a break in the regeneration of the Ca^{2+} wave and a space in which the Ca^{2+} signal can dissipate. Hypothetically introducing Ca^{2+} release sites within the gap has the effect of increasing both the velocity and amplitude of the centripetal Ca^{2+} wave (Fig. 3). These in silico results indicate that the gap in RyR expression is a structural feature to prevent inward movement of Ca^{2+}, and thereby reduce atrial energy use when hemodynamic requirements are low.

When hemodynamic demand increases, the atrial chambers make a significant contribution to ventricular refilling. Adrenergic stimulation is a key physiological mechanism for enhancing atrial contraction (1) (Fig. S4). The effect of adrenergic stimulation is largely mediated by the activation of protein kinase A (PKA), which has numerous putative targets within a cardiac myocyte. Notably, PKA-dependent phosphorylation causes an increase in VOC activity, which will lead to additional recruitment of dyadic junctions during EC coupling (analogous to changing the initial fraction). Furthermore, phosphorylation of the endogenous SERCA inhibitor phospholamban causes a marked elevation of SR Ca^{2+} content that both sensitizes RyRs for CICR and increases the flux of Ca^{2+} through RyRs upon their activation (analogous to changing threshold and release strength, respectively) (1). It is difficult to experimentally separate the contributions of increased VOC activity, reduced threshold for CICR, and increased Ca^{2+} flux. Our simulations indicated that all three parameters have the potential to gradually modulate the inotropic status of an atrial myocyte by determining the ability of centripetal Ca^{2+} waves to propagate from the periphery to the cell center (Fig. 4 and Fig. S3). Furthermore, the effect of these parameters on Ca^{2+} wave propagation was codependent. For example, altering the fraction of activated peripheral Ca^{2+} release sites at the onset of a response produced a steeply graded response in terms of centripetal Ca^{2+} wave propagation. Activating only a few of the peripheral Ca^{2+} release sites was generally insufficient to trigger a centripetal Ca^{2+} wave. However, increasing the Ca^{2+} release flux compensated for the lack of peripheral Ca^{2+} release site activation, and promoted centripetal Ca^{2+} waves (Fig. 4). Similarly, decreasing the threshold for CICR, to mimic RyR sensitization by SR Ca^{2+}, also supported centripetal Ca^{2+} waves. Our data indicate that multiple, interdependent processes determine the ability of centripetal Ca^{2+} waves to propagate, and thereby regulate contraction.

In addition to examining the factors underlying inotropy within atrial myocytes, we explored processes controlling the initiation and propagation of proarrhythmic Ca^{2+} waves. As described above, application of adrenergic agonists increases atrial myocyte inotropy, but also leads to the development of spontaneous Ca^{2+} signals (Fig. S5). A plausible explanation for such observations is stochastic activation of RyRs resulting from increased SR Ca^{2+} loading. We modeled this situation by changing the threshold at which cytosolic Ca^{2+} could activate Ca^{2+} release sites randomly in time. It is evident that increasing the spread of thresholds causes progressively more spontaneous Ca^{2+} wave generation (Fig. 7). In addition to RyRs, atrial myocytes express inositol 1,4,5-trisphosphate receptors ($InsP_3Rs$). We and others (2, 5, 14) have demonstrated that specific activation of $InsP_3Rs$ provokes the generation of arrhythmic Ca^{2+} signals. Inclusion of $InsP_3Rs$ within the present model can be mimicked by changing RyR threshold. Essentially, the stochastic activation of $InsP_3Rs$ triggers further RyR activity and Ca^{2+} waves via CICR. However, even within a deterministic model, where all of the Ca^{2+} release sites have the same threshold for CICR, it is possible to trigger self-sustaining autonomous Ca^{2+} waves, such as the Ca^{2+} waves illustrated in Fig. 5. It is evident that several parameters are critical in determining whether autonomous Ca^{2+} waves persist. Essentially, Ca^{2+} waves are triggered when the cytosolic Ca^{2+} concentration is greater than the threshold for CICR. This implies that increased Ca^{2+} release flux or decreased SERCA activity makes autonomous Ca^{2+} signals more likely to occur. A further critical parameter determining the propensity for spontaneous Ca^{2+} wave initiation is the period in which RyRs remain refractory after the previous Ca^{2+} release event (17). Reducing the refractory period increases the likelihood that cytosolic Ca^{2+} will not recover sufficiently before RyRs are ready to respond again (Fig. 5*B*). Furthermore, mismatches in refractoriness between neighboring Ca^{2+} release sites can cause the nucleation of Ca^{2+} waves. This is the situation underlying the ping waves presented in Fig. 6, where two counterrotating Ca^{2+} waves perpetually travel around a z disk. The ping wave persists because RyRs within the z disk are never simultaneously refractory. These data therefore suggest that situations in which atrial myocyte Ca^{2+} signaling is enhanced (i.e., increased Ca^{2+} release flux or reduced threshold for CICR) can give rise to proarrhythmic Ca^{2+} signals. However, in addition, the activation of RyRs under conditions of relatively weak Ca^{2+} flux also leads to proarrhythmic Ca^{2+} release activity due to nonsynchronous activation of RyRs and their refractory states.

The formation of ping waves is a clear prediction of our modeling framework, a Ca^{2+} pattern that could not have been resolved with current experimental techniques. Our approach allows us to probe the way in which Ca^{2+} activity between different z planes interacts and hence to unravel the complex contributions to physiological and pathological Ca^{2+} signals, which emphasizes the useful power of a computational cell biology approach to Ca^{2+} signaling.

Materials and Methods

The dynamics of Ca^{2+} concentration, $c(\mathbf{r}, t)$, $\mathbf{r} \in \mathbb{R}^3$, $t \in \mathbb{R}^+$, in the cylinder is governed by a generalization of the original fire-diffuse-fire model (18, 19):

$$\frac{\partial c}{\partial t} = D\Delta c - \frac{c}{\tau} + \sum_{n\in\Gamma}\sum_{m\in\mathbb{N}} \delta(\mathbf{r}-\mathbf{r}_n)\eta\left(t-T_n^m\right). \quad [1]$$

Here, D and Δ denote the effective diffusion coefficient for Ca^{2+} and the Laplace operator in cylindrical coordinates, respectively. We model SERCA pumps as homogeneously distributed linear sinks of strength τ. The double sum corresponds to Ca^{2+} liberation from the SR through RyR channels. The N_{rel} release sites are located at discrete positions $\mathbf{r}_n$, $n \in \Gamma = \{1, \ldots, N_{\mathrm{rel}}\}$, and $\eta(t)$ holds all details about the release shape, which we here take as $\eta(t) = \sigma\Theta(t)\Theta(t - t_{\mathrm{rel}})$. Ca^{2+} is released for a fixed time t_{rel} with a constant conductance σ, and $\Theta(x)$ represents the Heaviside step function, which equals 1 for $x \geq 0$ and 0 otherwise. The time T_n^m in Eq. **1** corresponds to the instant when the nth release site conducts Ca^{2+} for the mth time. The computation of the release times T_n^m renders Eq. **1** highly nonlinear, because the mth liberation is obtained implicitly by demanding that the Ca^{2+} concentration reaches the threshold value c_{th} at time T_n^m and that there is at least a refractory period of t_{ref} between successive release events. For a broader and more elaborate discussion of the model, we refer the reader to *SI Materials and Methods*.

ACKNOWLEDGMENTS. R.T. was supported through a Leverhulme Trust Early Career Fellowship. M.D.B. and H.L.R. were supported by the Biotechnology and Biological Sciences Research Council and British Heart Foundation H.L.R. is a Royal Society University Research Fellow.

1. Bers DM (2002) Cardiac excitation-contraction coupling. *Nature* 415(6868):198–205.
2. Bootman MD, Smyrnias I, Thul R, Coombes S, Roderick HL (2011) Atrial cardiomyocyte calcium signalling. *Biochim Biophys Acta* 1813:922–934.
3. Koivumäki JT, Korhonen T, Tavi P (2011) Impact of sarcoplasmic reticulum calcium release on calcium dynamics and action potential morphology in human atrial myocytes: A computational study. *PLoS Comput Biol* 7:e1001067.
4. Grandi E, et al. (2011) Human atrial action potential and Ca^{2+} model: Sinus rhythm and chronic atrial fibrillation. *Circ Res* 109:1055–1066.
5. Mackenzie L, et al. (2002) The role of inositol 1,4,5-trisphosphate receptors in Ca^{2+} signalling and the generation of arrhythmias in rat atrial myocytes. *J Physiol* 541: 395–409.
6. Woo SH, Cleemann L, Morad M (2002) Ca^{2+} current-gated focal and local Ca^{2+} release in rat atrial myocytes: Evidence from rapid 2-D confocal imaging. *J Physiol* 543: 439–453.
7. Sheehan KA, Blatter LA (2003) Regulation of junctional and non-junctional sarcoplasmic reticulum calcium release in excitation-contraction coupling in cat atrial myocytes. *J Physiol* 546(Pt 1):119–135.
8. Mackenzie L, Roderick HL, Berridge MJ, Conway SJ, Bootman MD (2004) The spatial pattern of atrial cardiomyocyte calcium signalling modulates contraction. *J Cell Sci* 117:6327–6337.
9. Bootman MD, Higazi DR, Coombes S, Roderick HL (2006) Calcium signalling during excitation-contraction coupling in mammalian atrial myocytes. *J Cell Sci* 119: 3915–3925.
10. Carl SL, et al. (1995) Immunolocalization of sarcolemmal dihydropyridine receptor and sarcoplasmic reticular triadin and ryanodine receptor in rabbit ventricle and atrium. *J Cell Biol* 129:673–682.
11. Chen-Izu Y, et al. (2006) Three-dimensional distribution of ryanodine receptor clusters in cardiac myocytes. *Biophys J* 91(1):1–13.
12. Kockskämper J, et al. (2001) Activation and propagation of Ca^{2+} release during excitation-contraction coupling in atrial myocytes. *Biophys J* 81:2590–2605.
13. Mackenzie L, Bootman MD, Berridge MJ, Lipp P (2001) Predetermined recruitment of calcium release sites underlies excitation-contraction coupling in rat atrial myocytes. *J Physiol* 530:417–429.
14. Bootman MD, Harzheim D, Smyrnias I, Conway SJ, Roderick HL (2007) Temporal changes in atrial EC-coupling during prolonged stimulation with endothelin-1. *Cell Calcium* 42:489–501.
15. Hille B (2001) *Ion Channels of Excitable Membranes* (Sinauer Associates, Sunderland, MA), 3rd Ed.
16. Izu LT, Means SA, Shadid JN, Chen-Izu Y, Balke CW (2006) Interplay of ryanodine receptor distribution and calcium dynamics. *Biophys J* 91(1):95–112.
17. Niggli E (2011) Ryanodine receptors: Waking up from refractoriness. *Cardiovasc Res* 91:563–564.
18. Keizer J, Smith GD, Ponce-Dawson S, Pearson JE (1998) Saltatory propagation of Ca^{2+} waves by Ca^{2+} sparks. *Biophys J* 75:595–600.
19. Coombes S, Timofeeva Y (2003) Sparks and waves in a stochastic fire-diffuse-fire model of Ca^{2+} release. *Phys Rev E Stat Nonlin Soft Matter Phys* 68:021915.